Adaptive Unscented Kalman Filter-based Disturbance Rejection With Application to High Precision Hydraulic Robotic Control

Peng Lu[1,2], Timothy Sandy[2] and Jonas Buchli[2]

***Abstract*— This paper presents a novel nonlinear disturbance rejection approach for high precision model-based control of hydraulic robots. While most disturbance rejection approaches make use of observers, we propose a novel adaptive Unscented Kalman Filter to estimate the disturbances in an unbiased minimum-variance sense. The filter is made adaptive such that there is no need to tune the covariance matrix for the disturbance estimation. Furthermore, whereas most model-based control approaches require the linearization of the system dynamics, our method is derivative-free which means that no linearization is required. Through extensive simulations as well as real hardware experiments, we demonstrate that our proposed approach can achieve high precision tracking and can be readily applied to most robotic systems even in the presence of uncertainties and external disturbances. The proposed approach is also compared to existing approaches which demonstrates its superior tracking performance.**

I. INTRODUCTION

Hydraulic actuators have a high power-to-weight ratio and can provide forces necessary for highly dynamic robots [1]. As such, robots driven by hydraulic actuators have shown impressive performance which might be difficult to achieve for those driven by electrical actuators. The hydraulic robot Atlas developed by Boston Dynamics can perform acrobatic motions which demonstrates the powerful performance of hydraulic actuators. However, hydraulic actuators are more difficult to control due to their complex dynamics. Even with internal force controllers, the closed-loop bandwidth of these actuators may be low, leading to unsatisfactory tracking. This is even more severe when the inertia of the link is low (such as the end effector of the robotic arm shown in Fig. 1). In this case, oil friction will also significantly degrade the tracking performance. Consequently, this limits their use in high precision tasks such as construction tasks [2].

To make these hydraulic robots able to achieve accurate tracking for high precision tasks, this paper explores model-based control techniques [3], [4], [5], [6]. On the one hand, these control techniques make use of the system dynamics to cancel the nonlinearities in the system model. On the other hand, it also leads to the problem of model uncertainties. Significant nonlinearities can be difficult to model. Additionally, external disturbances can be present which brings more challenge to model-based control techniques.

This research is funded by a Swiss National Science Foundation through the NCCR Digital Fabrication and a Professorship Award to Jonas Buchli

[1]Interdisciplinary Division of Aeronautical and Aviation Engineering, the Hong Kong Polytechnic University, HKSAR, China peng.lu@polyu.edu.hk

[2]Agile & Dexterous Robotics Lab at the Institute of Robotics and Intelligent Systems, ETH Zürich, Switzerland {tsandy and buchlij}@ethz.ch

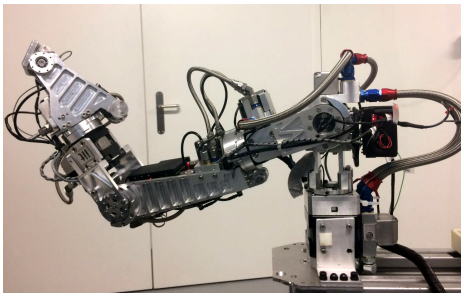

Fig. 1: The hydraulic arm used in the experiments.

Model-based control methods, such as optimal control [4], [7], inverse dynamics control [3], [8], [5], [6] and operational space control [9], [10], have been an active research in the field of robotics. While these approaches show great potential, their performance is degraded due to uncertainties in the system model. To deal with model uncertainties, nonlinear adaptive control [3], [11], [5], [6] is proposed. Adaptive control guarantees the system stability by updating the parameter estimate based on a Lyapunov design approach.

While adaptive control can cope with model uncertainties, its tracking performance can degrade in the presence of external disturbances. In the low-level actuator control of hydraulic robots such as the one shown in Fig. 1, the friction force in the actuators is difficult to estimate. Besides, robots could interact with external objects during operation. Carrying an unknown payload can also be seen as an external disturbance to the system. Robust control can cope with model uncertainty since it is designed by taking account of the worst scenario including failures; thus limiting its performance when the system is operating nominally. Sliding mode control [12] is proposed to deal with disturbances. But it requires the bounds of the disturbance and its derivative which are difficult to obtain in practice.

Another way to cope with disturbances is through disturbance observers [13], [14], [15], [16]. However, most of these approaches need to linearize the rigid body dynamics or do not consider the sensor noise.

Although many model-based approaches can cope with nonlinear systems [17], [18], [19], they still rely on the linearization of the system model. In robotics, while these derivatives are difficult to obtain analytically [20], many differentiation methods are proposed. However, the computational load increases significantly when the number of Degrees-Of-Freedom (DOF) increases. This poses a chal-

lenge to real time applications.

In this paper, a novel disturbance rejection control is proposed to improve the tracking performance of hydraulic robotic arms. It is assumed that the hydraulic actuators have internal force controllers but the force tracking is unsatisfactory. The proposed method models both model uncertainties and external disturbances as total disturbances. Then, a newly-developed adaptive Unscented Kalman Filter (UKF) is presented to estimate the total disturbances online. Finally, the unbiased estimates of the disturbances are used by the controller to attenuate the influence of the disturbances.

The contributions of this paper are as follows:

1) The method we propose is nonlinear unlike many other approaches using observers which need to linearize the system dynamics.
2) A novel adaptive UKF is proposed. When UKF[21] is used to estimate disturbances, the disturbances are augmented as the states and can be modeled as random walk processes. However, the covariance matrix of the random walk processes is unknown. In this paper, we propose a novel adaptive UKF which can update the covariance of the disturbance estimation error adaptively based on the innovation covariance matching. In this case, there is no need to tune the covariance matrix for disturbance estimation.
3) To the best of our knowledge, this is the first paper which makes use of an adaptive UKF for disturbance rejection control. It can achieve unbiased minimum-variance estimate even in the presence of sensor noise.
4) This is one of the few papers which experimentally demonstrate that the proposed method can significantly improve the tracking performance of *hydraulic* robots.

To demonstrate the superior performance and generality of the proposed approach, we validate our approach on different platforms (a hydraulic arm and a hydraulic quadruped) as well as in different disturbance situations (unmodelled actuator dynamics and abruptly dropped weight). Furthermore, we compare our approach with high gain controllers as well as recent disturbance attenuation approach in literature.

The structure of this paper is as follows: Section II presents the nominal model and perturbed model with model uncertainties and disturbances. Section III proposes the adaptive and simplified UKF which can estimate the disturbances online. The overall controller is shown in SectionIV. The performance tests in simulation are given in Section V and experimental tests are given in Section VI. Finally, Section VII concludes the paper and proposes future research.

II. Nominal and perturbed model of the robots

This section first presents the nominal model of the rigid body dynamics. Then, the perturbed model, which contains model uncertainties and external disturbances is presented.

A. Rigid body dynamics

Consider the rigid-body dynamics with the following equations of motion:

$$\mathbf{M}(\boldsymbol{q})\ddot{\boldsymbol{q}} + \mathbf{C}(\boldsymbol{q}, \dot{\boldsymbol{q}}) + \mathbf{G}(\boldsymbol{q}) = \boldsymbol{\tau} \tag{1}$$

with $\boldsymbol{q}$ is the $n_d \times 1$ vector of joint angular positions with n_d the number of DOF, $\mathbf{M}(\boldsymbol{q})$ the $n_d \times n_d$ inertia matrix, $\mathbf{C}(\boldsymbol{q}, \dot{\boldsymbol{q}})$ the $n_d \times 1$ Coriolis and centripetal torques and $\mathbf{G}(\boldsymbol{q})$ the $n_d \times 1$ gravitational torques. $\boldsymbol{\tau}$ is $n_d \times 1$ vector of joint torques. For the sake of readability, the dependencies of the system matrices $\mathbf{M}(\boldsymbol{q})$, $\mathbf{C}(\boldsymbol{q}, \dot{\boldsymbol{q}})$ and $\mathbf{G}(\boldsymbol{q})$ on $\boldsymbol{q}$ and $\dot{\boldsymbol{q}}$ will be discarded and the system dynamics are rewritten as:

$$\ddot{\boldsymbol{q}} = -\mathbf{M}^{-1}(\mathbf{C} + \mathbf{G}) + \mathbf{M}^{-1}\boldsymbol{\tau} \tag{2}$$

B. Rigid body dynamics with model uncertainties and disturbances

Practically, it is difficult to obtain the exact system parameters, which leads to model uncertainties ($\Delta\mathbf{M}$, $\Delta\mathbf{C}$ and $\Delta\mathbf{G}$). Even with internal force controllers, the tracking of hydraulic actuators is not satisfactory especially when the joint inertia is low. Oil friction also significantly degrades the tracking performance, which leads to torque uncertainties. Additionally, external disturbances also bring uncertain torques. All the uncertainties related to the torque command are denoted as $\Delta\boldsymbol{\tau}$. Taking the uncertainties and external disturbances into account, the system dynamics Eq. (1) is rewritten into the following:

$$\mathbf{M}\ddot{\boldsymbol{q}} + \Delta\mathbf{M}\ddot{\boldsymbol{q}} + \mathbf{C} + \Delta\mathbf{C} + \mathbf{G} + \Delta\mathbf{G} = \boldsymbol{\tau} + \Delta\boldsymbol{\tau} \tag{3}$$

where $\mathbf{M}$, $\mathbf{C}$ and $\mathbf{G}$ are calculated based on the method in [22]. Now we can also write the above system into the same form with Eq. (2) as follows:

$$\ddot{\boldsymbol{q}} = -\mathbf{M}^{-1}(\mathbf{C} + \mathbf{G}) + \mathbf{M}^{-1}\boldsymbol{\tau} + \boldsymbol{d} \tag{4}$$

where $\boldsymbol{d}$ denotes the total disturbances. Note that lumping all uncertainties and disturbance as $\boldsymbol{d}$ has been used in disturbance observer-based approaches to achieve disturbance rejection [13], [14], [15], [16]. However, these approaches either linearize the system dynamics or do not consider the noise. In this paper, we will propose a novel method which does not linearize the system dynamics and can achieve unbiased minimum-variance estimate in the presence of sensor noise.

III. Estimation of total disturbances

This section presents the novel approach which estimate the total disturbance $\boldsymbol{d}$ in an unbiased minimum-variance sense. First, the disturbance estimate using the UKF is presented. Then, a simplified UKF is proposed to reduce the sigma point calculation. Finally, a novel adaptive UKF is proposed.

A. Process and measurement models for disturbance estimation

To use the UKF for disturbance estimate, the process and measurement models need to be presented first. The process model can be readily obtained from the system dynamics model denoted in Eq. (4). Let the state of the filter be

$$\boldsymbol{x} = [\boldsymbol{x}_1, \boldsymbol{x}_2, \boldsymbol{x}_3]^T \tag{5}$$

with $\boldsymbol{x}_1 = \boldsymbol{q}, \boldsymbol{x}_2 = \dot{\boldsymbol{q}}, \boldsymbol{x}_3 = \boldsymbol{d}$. Then the process model can be given as follows:

$$\dot{\boldsymbol{x}} = \boldsymbol{f} + \boldsymbol{g}\boldsymbol{u} + \mathbf{E}\boldsymbol{w}_d \tag{6}$$

where

$$\boldsymbol{f} = \begin{bmatrix} \boldsymbol{x}_2 \\ -\mathbf{M}^{-1}(\mathbf{C}+\mathbf{G}) + \boldsymbol{d} \\ \mathbf{0} \end{bmatrix} \tag{7}$$

$$\boldsymbol{g} = \begin{bmatrix} \mathbf{0} \\ \mathbf{M}^{-1} \\ \mathbf{0} \end{bmatrix}, \mathbf{E} = \begin{bmatrix} \mathbf{0} \\ \mathbf{I} \\ \mathbf{I} \end{bmatrix}, \boldsymbol{u} = \boldsymbol{\tau} \tag{8}$$

Note here we model the dynamics of $\boldsymbol{d}$ as a random walk process [23]. $\boldsymbol{w}_d$ is a white noise sequence with zero mean and covariance $\mathbf{Q}_d$ with $E\{\boldsymbol{w}_{d,k}\boldsymbol{w}_{d,l}^T\} = \mathbf{Q}_d\delta_{kl}$.

The measurement model can be obtained based on the available sensors. In our work, only joint angle sensors and torque sensors are available. Therefore, the measurement model can be given by:

$$\boldsymbol{y}_m = \boldsymbol{h}(\boldsymbol{x}) + \boldsymbol{v} = \boldsymbol{x}_1 + \boldsymbol{v} \tag{9}$$

$$= [\mathbf{I}, \mathbf{0}, \mathbf{0}]\boldsymbol{x} + \boldsymbol{v} \tag{10}$$

$$:= \mathbf{H}\boldsymbol{x} + \boldsymbol{v} \tag{11}$$

where $\boldsymbol{v}$ is the measurement noise vector which is assumed to be a white noise with covariance $\mathbf{R}$ defined by $E\{\boldsymbol{v}_k\boldsymbol{v}_l^T\} = \mathbf{R}\delta_{kl}$. $\mathbf{R}$ is determined by the sensors (joint encoders).

B. Disturbance estimation using UKF

At time step k, the estimate using the UKF can be done through the following steps:

1) Sigma points calculation

$$\mathcal{X}_{k-1} = [\hat{\boldsymbol{x}}_{k-1}, \hat{\boldsymbol{x}}_{k-1} - \gamma\sqrt{\mathbf{P}_{k-1}}, \hat{\boldsymbol{x}}_{k-1} + \gamma\sqrt{\mathbf{P}_{k-1}}] \tag{12}$$

where $\mathcal{X}_{i,k-1}$ are the sigma points of the states $\boldsymbol{x}$ (with dimension $n = 3n_d$) at step $k-1$. $\gamma = \sqrt{n+\lambda}$. $\lambda = \alpha^2(n+\kappa) - n$ with $\kappa = 0$, $\alpha = 0.8$ and $\beta = 2$. $\hat{\boldsymbol{x}}_{k-1}$ and $\mathbf{P}_{k-1}$ are the state estimation and its error covariance matrix at time step $k-1$.

2) Time update
After the calculation of the sigma points, the predicted mean $\hat{\boldsymbol{x}}_{k|k-1}$ and its error covariance matrix $\mathbf{P}_{k|k-1}$ are computed as follows:

$$\mathcal{X}^*_{i,k|k-1} = \mathcal{X}_{i,k-1} + \int_{t_{k-1}}^{t_k} \boldsymbol{f}(\mathcal{X}_{i,k-1}, \boldsymbol{u}(\tau), \tau)d\tau \tag{13}$$

$$\hat{\boldsymbol{x}}_{k|k-1} = \sum_{i=0}^{2n} W_i^{(m)}\mathcal{X}^*_{i,k|k-1} \tag{14}$$

$$\mathbf{P}_{k|k-1} = \mathbf{Q}_c + \boldsymbol{P}^*_{k|k-1} \tag{15}$$

where $\boldsymbol{P}^*_{k|k-1} = \sum_{i=0}^{2n} W_i^{(c)}[\mathcal{X}^*_{i,k|k-1} - \hat{\boldsymbol{x}}_{k|k-1}][\mathcal{X}^*_{i,k|k-1} - \hat{\boldsymbol{x}}_{k|k-1}]^T)$. $\hat{\boldsymbol{x}}_{k|k-1}$ and $\mathbf{P}_{k|k-1}$ are the predicted state and its error covariance matrix. $\mathbf{Q}_c = \int_{t_{k-1}}^{t_k} \mathbf{E}\mathbf{Q}_d\mathbf{E}^T dt$ and is approximated by $\mathbf{E}\mathbf{Q}_d\mathbf{E}^T\Delta t$ where $\Delta t = t_k - t_{k-1}$. Redraw sigma points as follows[1]

$$\mathcal{X}_{k|k-1} = [\hat{\boldsymbol{x}}_{k|k-1}, \hat{\boldsymbol{x}}_{k|k-1} - \gamma\sqrt{\mathbf{P}_{k|k-1}}, \hat{\boldsymbol{x}}_{k|k-1} + \gamma\sqrt{\mathbf{P}_{k|k-1}}] \tag{16}$$

then

$$\mathcal{Y}_{i,k|k-1} = \boldsymbol{h}(\mathcal{X}_{i,k|k-1}) \tag{17}$$

$$\hat{\boldsymbol{y}}_k = \sum_{i=0}^{2n} W_i^{(m)}\mathcal{Y}_{i,k|k-1} \tag{18}$$

$$\mathbf{P}_{xy,k} = \sum_{i=0}^{2n} W_i^{(c)}[\mathcal{X}_{i,k|k-1} - \hat{\boldsymbol{x}}_{k|k-1}][\mathcal{Y}_{i,k|k-1} - \hat{\boldsymbol{y}}_k]^T \tag{19}$$

$$\mathbf{P}_{yy,k} = \sum_{i=0}^{2n} W_i^{(c)}[\mathcal{Y}_{i,k|k-1} - \hat{\boldsymbol{y}}_k][\mathcal{Y}_{i,k|k-1} - \hat{\boldsymbol{y}}_k]^T + \mathbf{R} \tag{20}$$

$W_i^{(m)}$ and $W_i^{(c)}$, which are the weights associated with the ith point with respect to $\hat{\boldsymbol{x}}_{k-1}$ and $\mathbf{P}_{k-1}$, are calculated according to [24].

3) Measurement update

$$\mathbf{K}_k = \mathbf{P}_{xy,k}\mathbf{P}^{-1}_{yy,k} \tag{21}$$

$$\boldsymbol{\gamma}_k = \boldsymbol{y}_{m,k} - \hat{\boldsymbol{y}}_k \tag{22}$$

$$\hat{\boldsymbol{x}}_k = \hat{\boldsymbol{x}}_{k|k-1} + \mathbf{K}_k\boldsymbol{\gamma}_k \tag{23}$$

$$\mathbf{P}_k = \mathbf{P}_{k|k-1} - \mathbf{K}_k\mathbf{P}_{yy,k}\mathbf{K}_k^T \tag{24}$$

where $\boldsymbol{y}_{m,k}$ is the measurement at time step k. $\boldsymbol{\gamma}_k$ is the innovation and $\mathbf{K}_k$ is the Kalman gain of the filter. $\hat{\boldsymbol{x}}_k$ and $\mathbf{P}_k$ are the final state estimate and estimation error covariance matrix. They are used as the prior knowledge for the next time step $(k+1)$ as in Eq. (12).

C. Disturbance estimation using Simplified UKF

The UKF is less sensitive to initialization errors and linearization errors unlike its counterpart Extended Kalman Filter (EKF). Furthermore, the UKF does not require the linearization of the system matrices while the EKF must calculate the Jacobian matrices of the system models. However, the UKF requires the calculation of sigma points. In this section, we will reduce the calculation of sigma points to simplify the UKF.

Due to the fact that the measurement model is linear, Eq. (17) can be written as:

$$\mathcal{Y}_{i,k|k-1} = \mathbf{H}\mathcal{X}_{i,k|k-1} \tag{25}$$

Similarly, Eq. (18) can be written as:

$$\hat{\boldsymbol{y}}_k = \sum_{i=0}^{2n} W_i^{(m)}\mathbf{H}\mathcal{X}_{i,k|k-1} \tag{26}$$

[1]See Page 233 of [24]

Note that the mean of the redrawn sigma points $\mathcal{X}_{k|k-1}$ is still $\hat{\boldsymbol{x}}_{k|k-1}$. Therefore, Eq. (26) reduces to

$$\hat{\boldsymbol{y}}_k = \mathbf{H}\hat{\boldsymbol{x}}_{k|k-1} \tag{27}$$

Substituting Eq. (25) and (27) into Eq. (19), we obtain

$$\mathbf{P}_{xy,k} = \sum_{i=0}^{2n} W_i^{(c)}[\mathcal{X}_{i,k|k-1} - \hat{\boldsymbol{x}}_{k|k-1}][\mathcal{X}_{i,k|k-1} - \hat{\boldsymbol{x}}_{k|k-1}]^T\mathbf{H}^T \tag{28}$$

Since $\sum_{i=0}^{2n} W_i^{(c)}[\mathcal{X}_{i,k|k-1} - \hat{\boldsymbol{x}}_{k|k-1}][\mathcal{X}_{i,k|k-1} - \hat{\boldsymbol{x}}_{k|k-1}]^T$ is the covariance matrix of sigma points $\mathcal{X}_{k|k-1}$, Eq. (28) reduces to

$$\mathbf{P}_{xy,k} = \mathbf{P}_{k|k-1}\mathbf{H}^T \tag{29}$$

Likewise, Eq. (20) reduces to

$$\mathbf{P}_{yy,k} = \mathbf{H}\mathbf{P}_{k|k-1}\mathbf{H}^T + \mathbf{R} \tag{30}$$

Now, we can give the *simplifications* to the UKF:

Simplifications for the UKF

Replace Eqs. (16)-(20) with
Eqs. (27), (29) and (30).

Eqs. (27), (29) and (30) have the same form as that of the EKF. This is reasonable since our measurement model is linear and there is no need to calculate the sigma points to approximate the nonlinear function. The benefits of the simplifications are as follows:

1) Fewer calculations of sigma points. The sigma points calculations for the measurement model and covariance matrices are removed.
2) Free of linearization or derivatives. The EKF requires the linearization of the system matrices $\boldsymbol{f}$ to get its derivative with respect to $\boldsymbol{x}$. In this paper, the dimension of $\boldsymbol{x}$ is $3n_d$ with n_d the number of DOF. As these derivatives are difficult to derive analytically, numerical differentiation and auto-differentiation methods are usually used to reduce the computational load. In contrast, the UKF does not need any of this.

Based on these benefits, the simplified UKF seems to be a more suitable choice than the EKF. In the following section, we will also make use of this simplified UKF to derive the Adaptive Unscented Kalman Filter (AUKF).

D. Novel Adaptive Unscented Kalman Filter

Since the dynamics of $\boldsymbol{d}$ is unknown, it is modeled as a random walk process driven by the covariance matrix $\mathbf{Q}_d$. Therefore, the choice of $\mathbf{Q}_d$ is of critical importance. Due to the unknown behavior of $\boldsymbol{d}$, it is difficult to determine $\mathbf{Q}_d$. An ad hoc solution is to manually tune it in simulation and then apply it in practice. We will propose a novel method to adaptively update $\mathbf{Q}_d$.

Substituting Eq. (15) into Eq.(30), the innovation covariance matrix $\mathbf{P}_{yy,k}$ is expressed as:

$$\mathbf{H}(\mathbf{Q}_c + \boldsymbol{P}^*_{k|k-1})\mathbf{H}^T + \mathbf{R} \tag{31}$$

The actual innovation covariance can be approximated by:

$$\hat{\mathbf{C}}_k = \frac{1}{N}\sum_{j=k-N+1}^{k} \boldsymbol{\gamma}_j\boldsymbol{\gamma}_j^T \tag{32}$$

where $\boldsymbol{\gamma}_j$ is defined in Eq. (22). It should be noted that if the angular rates $\dot{\boldsymbol{q}}$ are also measured, $\mathbf{H} = [\mathbf{I}, \mathbf{I}, \mathbf{0}]^T$, we can obtain the following based on the matching of the innovation covariances:

$$\mathbf{H}\mathbf{E}\mathbf{Q}_d\mathbf{E}^T\mathbf{H}^T\Delta_t = \hat{\mathbf{C}}_k - \mathbf{H}\boldsymbol{P}^*_{k|k-1}\mathbf{H}^T - \mathbf{R}. \tag{33}$$

Although $\mathbf{H}$ and $\mathbf{E}$ are not directly invertible, $\mathbf{H}\mathbf{E} = \mathbf{I}$ is invertible. Consequently, the left side of Eq. (33) is simplified into $\mathbf{Q}_d\Delta_t$ and $\mathbf{Q}_d$ is obtained as:

$$\mathbf{Q}_d = (\hat{\mathbf{C}}_k - \mathbf{H}\boldsymbol{P}^*_{k|k-1}\mathbf{H}^T - \mathbf{R})/\Delta_t. \tag{34}$$

However, in our experiments, there are no available sensors to measure $\dot{\boldsymbol{q}}$ and we can only approximate $\mathbf{Q}_d$ by Eq. (34). It will be illustrated by simulations and experiments that this approximation can achieve satisfactory results.

By now all the parameters for the UKF have been determined and the unbiased disturbance estimates at time step k are obtained by $\hat{\boldsymbol{x}}_{2n_d+1:3n_d,k}$.

IV. Model-based controller design

In this section, we will present the model-based controller without and with the disturbance rejection.

A. Controller without disturbance rejection

In this subsection, we assume $\boldsymbol{d} = 0$, which means we do not consider the disturbances. The control law is designed based on inverse dynamics control, also known as *computed torque control* [5], [6], [8].

Define the tracking error vector $\boldsymbol{e}$ as $\boldsymbol{e} = \boldsymbol{q} - \boldsymbol{q}_{des}$ and the derivative of $\boldsymbol{e}$ as $\dot{\boldsymbol{e}} = \dot{\boldsymbol{q}} - \dot{\boldsymbol{q}}_{des}$ where the subscript "des" denotes the desired reference command. The control law is designed as follows:

$$\boldsymbol{\tau} = \mathbf{C} + \mathbf{G} + \mathbf{M}(\ddot{\boldsymbol{q}}_{des} - \mathbf{K}_D\dot{\boldsymbol{e}} - \mathbf{K}_P\boldsymbol{e}) \tag{35}$$

where $\mathbf{K}_P$ and $\mathbf{K}_D$ are the proportional and derivative gains.

B. Controller with disturbance rejection

The control law with disturbance rejection is designed as follows:

$$\boldsymbol{\tau} = \mathbf{C} + \mathbf{G} + \mathbf{M}(\ddot{\boldsymbol{q}}_{des} - \mathbf{K}_D\dot{\boldsymbol{e}} - \mathbf{K}_P\boldsymbol{e} - \hat{\boldsymbol{d}}) \tag{36}$$

where $\hat{\boldsymbol{d}}$ is the estimate of $\boldsymbol{d}$.

The block diagram of the control system is shown in Fig. 2. The reference block provides the information of the desired reference $\boldsymbol{q}_{des}$, $\dot{\boldsymbol{q}}_{des}$ and $\ddot{\boldsymbol{q}}_{des}$. It is seen from the block diagram that the AUKF takes the torque command and the sensor measurements as input. The output of the AUKF, which is the unbiased estimate of $\boldsymbol{d}$, is fed to the controller to attenuate the effect of $\boldsymbol{d}$ based on control law Eq. (36). The performance of this approach will be validated in the following sections.

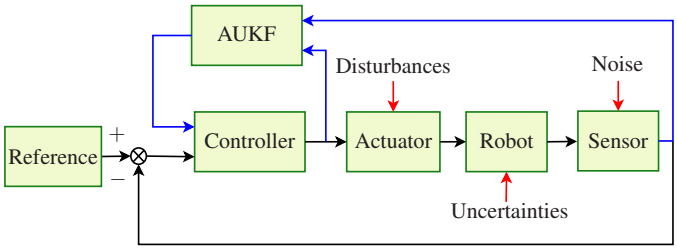

Fig. 2: Block diagram of the disturbance rejection controller. The reference block provides the desired reference commands $\boldsymbol{q}_{des}$, $\dot{\boldsymbol{q}}_{des}$ and $\ddot{\boldsymbol{q}}_{des}$ which are used by the control law Eq. (36).

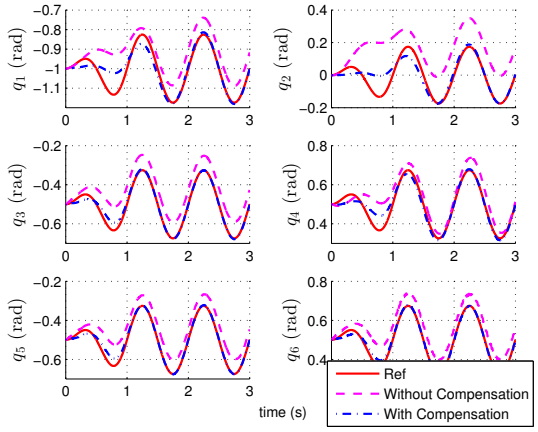

Fig. 3: Tracking of $\boldsymbol{q}_{des}$ using the controller *without* and *with* disturbance rejection.

V. Simulation Results

In this section, the tracking performance of the proposed method will be validated. Different validation platforms are used to test the generality to various systems.

A. A hydraulic arm-HyA

The robotic arm (shown in Fig. 1) has 6 DOF and each joint is driven by a hydraulic actuator. The joints are numbered from the shoulder to the wrist. A more detailed description of the design can be found in [1]. Although the bandwidths of the valves are high, the bandwidths of the closed-loop low-level actuator controllers are low[25]. In addition, there are significant friction forces in the actuators, which lead to the biases and delays in the actuator responses. We model this effect in a Gazebo simulation and use our proposed controller to deal with this issue. More specifically, we model the dynamics of the actuators as second-order low pass filters with damping ratio of 0.8 and natural frequency of 250 rad/s. Furthermore, we add biases ($[5, 10, 4, 4, 2, 2]^T Nm$) to the six actuators.

Fig. 3 shows the tracking performance using the controllers *without* and *with* disturbance rejection. It is seen that the controller *without* disturbance rejection is not able to follow the reference. There are biases in the tracking due to the added biases in the actuators. On the contrary, the controller *with* disturbance rejection converges to the desired reference closely. This demonstrates that the proposed controller can handle disturbances caused by the imperfect actuator dynamics.

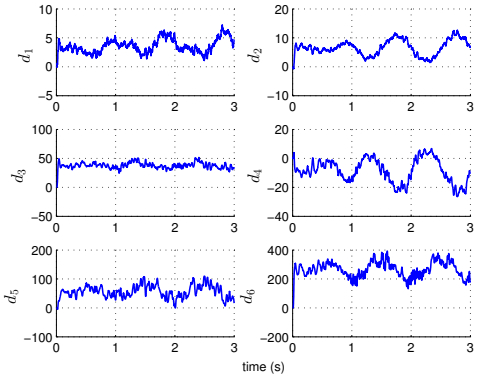

Fig. 4: Estimate of $\boldsymbol{d}$ using the AUKF for the HyA simulation. Note that the unit of $\boldsymbol{d}$ is rad/s^2.

The estimated disturbances for each joints are shown in Fig. 4. The added biases are constant but the estimated total disturbances are time-varying because the total disturbances also estimate the uncertainties caused by the actuator dynamics. These time-varying disturbances indeed pose a challenge to most model-based control approaches. Note that the unit of $\boldsymbol{d}$ is not Nm but rad/s^2. It is straightforward to derive the disturbance in terms of torque by multiplying $\boldsymbol{d}$ with $\mathbf{M}$.

B. A hydraulic quadrupedal robot-HyQ

This test is performed on a more complex robot: a quadrupedal robot [26], [25]. This robot has four legs (Left Front (LF), Left Hind (LH), Right Front (RF), Right Hind (RH)), each with three DOF (hip abduction/adduction (HAA), hip flexion/extension (HFE), knee flexion/extension (KFE) respectively). Taking the base position and orientation into consideration, there are 12 more DOF. In this section, we only consider the joint space control and we consider the force from the base and contact forces as external disturbances. This results in significant disturbances into the joint space system model as shown in Eq. (1). The controlled variables are the joint angular positions and velocities. The control task is that knee joints have to follow a sine trajectory while other joints maintain their positions. The simulation is performed in SL [27] which is a software package for complex rigid-body dynamics simulations.

To demonstrate the disturbance rejection performance of our approach, we add additional disturbances to each joint. For all the hip joints, the added torque disturbances are 10 Nm. The added disturbances to front knee joints are -50 Nm while those added to hind knee joints are 50 Nm.

Both controllers are tested when there are no additional disturbances and they are both working. The one with disturbance rejection has a better tracking performance. The reason is that the base gravity and contact forces bring unmodelled dynamics and are compensated by the disturbance estimate.

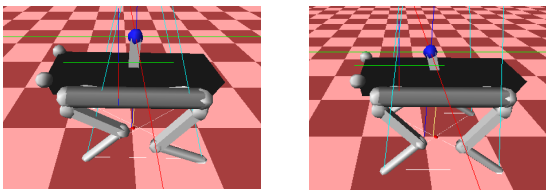

Fig. 5: Left and right subfigures show the results of using the controllers *without* and *with* disturbance rejection respectively. It is seen that hind knee joints of left subfigure drop. The knee joints go out of range and triggered the emergence stop. The right subfigure finished the task successfully.

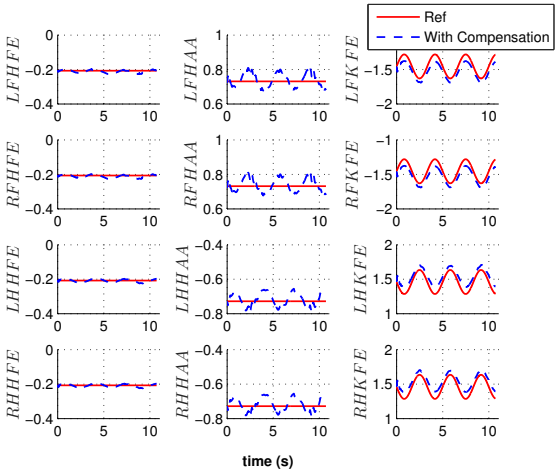

Fig. 6: Tracking of $\boldsymbol{q}_{des}$ using the controller *with* disturbance rejection for the HyQ simulation.

Then two controllers are tested with the additional disturbances added to each joint. The knee joints of using the controller *without* disturbance rejection go out of range and triggered the emergence stop, which is shown in the left subfigure of Fig. 5.

Contrarily, the controller *with* disturbance rejection successfully finished the task (shown in right subfigure of Fig. 5). The joint position tracking is shown in Fig. 6. The disturbance estimates are shown in Fig. 7. It can be observed that the disturbances are of big magnitudes, which result in the poor performance using the controller *without* disturbance rejection. However, the purpose of adding such big torque disturbances is to test when the controller *without* disturbance rejection will fail to work while the other controller still works well.

VI. Experimental Results

In this section, we apply our approach to our Hydraulic arm (HyA) hardware. Currently an inverse dynamics controller (control law Eq. (35)) with large PID gains is implemented to cope with the significant disturbance in the actuators. In this section, we test our new approach (control law Eq. (36) with AUKF) on this robotic arm. In the

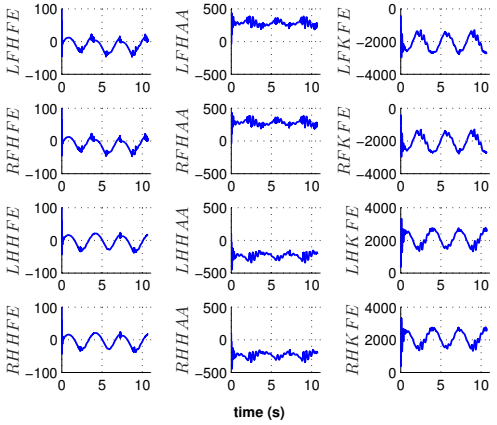

Fig. 7: Estimate of $\boldsymbol{d}$ (units in rad/s^2) using the AUKF for the HyQ simulation.

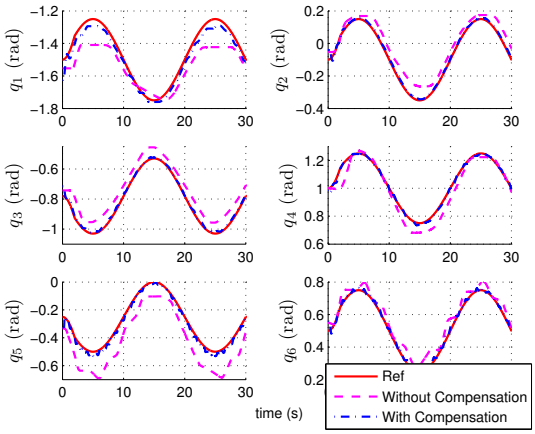

Fig. 8: Tracking of q_{des} using the controller *without* and *with* disturbance rejection during the HyA experiments, with gains in (37).

experiments, the following gains are used:

$$\mathbf{K}_P = \text{diag}(65, 60, 50, 60, 35, 35),$$
$$\mathbf{K}_D = \text{diag}(4, 4, 3.5, 3.5, 2, 2) \qquad (37)$$

It should be noted that the gains are tuned first in simulation and then tuned in real hardware. $\mathbf{K}_D$ is tuned relatively smaller to avoid magnifying the noise effect.

A. Experiments in the case of unmodeled actuator dynamics

The task of this experiment is that each joint has to follow a sine trajectory. The main disturbances include friction forces and unmodeled actuator dynamics. First, the results of the control laws (35) and (36) using the above gains are shown in Fig. 8. It is seen that the controller with disturbance rejection can track the reference closely while the other controller can not. For joint 1 using the one without compensation, it is stuck at -1.4 rad during $3 < t < 7$ s and $23 < t < 27$ s. The possible cause is the large friction force which limits the motion of the joint. The absolute tracking

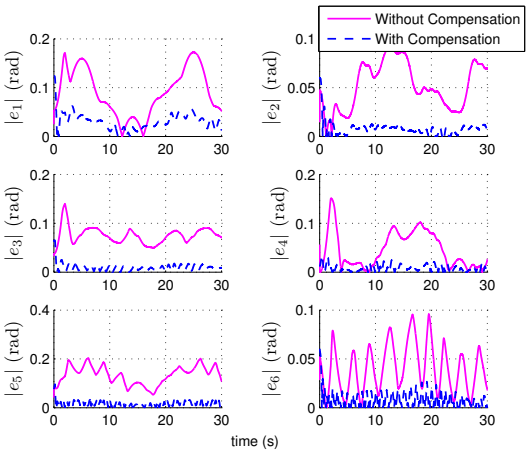

Fig. 9: Comparison of $|e|$ using the controller *without* and *with* disturbance rejection during the HyA experiments.

TABLE I: Comparison of root-mean squared tracking errors

	e_1	e_2	e_3	e_4	e_5	e_6
Without rejection	0.106	0.055	0.077	0.062	0.138	0.047
High gain	0.046	0.032	0.031	0.025	0.059	0.022
[16]	0.043	0.021	0.028	0.020	0.023	0.018
[28]	0.041	0.018	0.023	0.015	0.020	0.014
With rejection	0.031	0.010	0.011	0.010	0.016	0.011

errors of the two controllers are compared in Fig. 9. The absolute tracking errors using the controller with disturbance rejection are nearly always significantly smaller than the other controller.

The estimated $\boldsymbol{d}$ using the AUKF are shown in Fig. 10. It should be noted that the units of $\boldsymbol{d}$ is rad/s^2 instead of Nm. It is seen that the shape of $\boldsymbol{d}$ resembles that of the joint motion. Some oscillations are observed related to the last two joints. That is caused by the actuators whose closed-loop bandwidth is significantly reduced with low load.

To demonstrate the superiority of the proposed approach, we compare with three more approaches: one is control law (35) with high gains which are three times of those in (37) and the other one proposed in [16] and [28]. The first one (high gain) is usually used in control of hydraulic robots to cope with low tracking performance of hydraulic actuators. The one in [28] is a recently-developed method which shows advantages over most existing robust controllers or disturbance observer-based approaches in the presence of sensor noise (see [28] for more details). The root-mean squared errors (RMSE) of the tracking is shown in Table I. As seen, the tracking performance of the proposed approach outperforms the high-gain inverse dynamics control as well as the one in [16] and [28]. The reason why the one in [28] performs slightly worse is that it uses low pass filters which introduce delays in the disturbance estimate.

B. Experiments in the case of external disturbances

The approach is also tested in real hardware by abruptly dropping a weight to the end effector. Snapshots of using

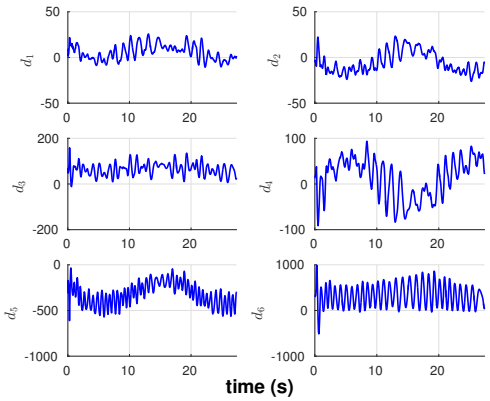

Fig. 10: Estimate of $\boldsymbol{d}$ (units in rad/s^2) using the AUKF during the HyA experiments.

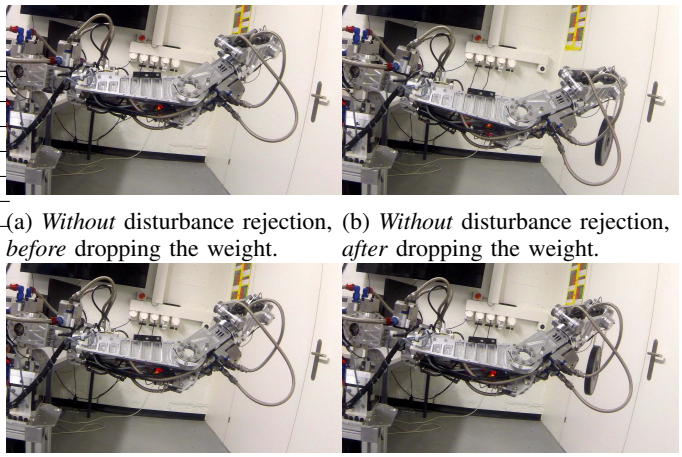

(a) *Without* disturbance rejection, *before* dropping the weight.

(b) *Without* disturbance rejection, *after* dropping the weight.

(c) *With* disturbance rejection, *before* dropping the weight.

(d) *With* disturbance rejection, *after* dropping the weight.

Fig. 11: Snapshots of the end effector positions.

the controller *without* disturbance rejection before and after dropping the weight are shown in Figs. 11a and 11b while those of using the controller *with* disturbance rejection are shown in Figs. 11c and 11d. It is observed that the end effector using the controller *with* disturbance rejection maintains its position while that using the other controller does not.

The tracking using the two controllers are shown in Fig. 12. The position of joint 2 and 4 using the one without disturbance rejection both drop after the weight is dropped to the end effector. Using the AUKF, the disturbances caused by the dropped weight are estimated (shown in Fig. 13). Note that the disturbance are multiplied with $\mathbf{M}$ for understanding how much torque are caused by the disturbance. A number of experiments are performed and the results are all similar. For instance, we also performed adding a weight while each joint has to follow a sine reference. Interested readers could refer to the video[2] for more details.

[2]https://youtu.be/vbLFAUgVE8A

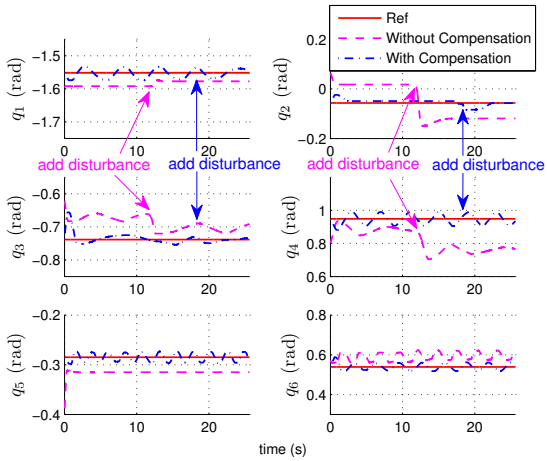

Fig. 12: Tracking of q_{des} using the controller *without* and *with* disturbance rejection during the HyA experiments with external disturbances, with gains in (37).

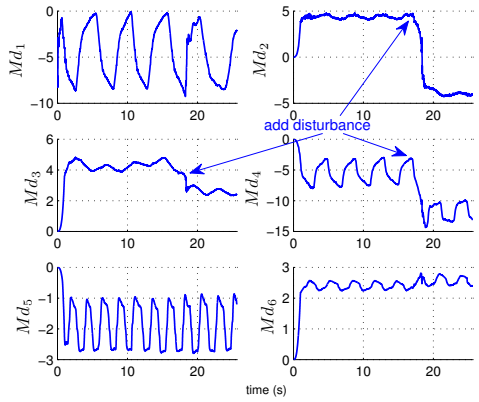

Fig. 13: Estimated $\mathbf{Md}$ (Nm) using the AUKF during the HyA experiments with external disturbances. The dropped weight introduced additional unknown torques. For instance, the total torque disturbance in joint 2 changes from 4.8 Nm to -4.8 Nm due to the added weight.

VII. CONCLUSIONS

This paper proposed a novel disturbance rejection control method for hydraulic robots. It takes model uncertainties and external disturbances into account. A novel Adaptive Unscented Kalman Filter was proposed to achieve an unbiased minimum-variance estimate of the total disturbance in real time even in the presence of sensor noise. Extensive experiments have demonstrated the superior tracking performance of the proposed approach over existing approaches.

The proposed approach can be readily extended to other robotic platforms. This approach can also be extended to design the internal force controller for hydraulic actuators.

REFERENCES

[1] B. U. Rehman, M. Focchi, M. Frigerio, J. Goldsmith, G. Darwin, and C. Semini, "Design of a Hydraulically Actuated Arm for a Quadruped Robot," in *Proceedings of the International Conference on Climbing and Walking Robots (CLAWAR)*, 2015.

[2] T. Sandy, M. Giftthaler, K. Dorfler, M. Kohler, and J. Buchli, "Autonomous Repositioning and Localization of an In situ Fabricator," in *IEEE International Conference on Robotics and Automation (ICRA)*, 2016, pp. 2852–2858.

[3] H. K. Khalil, *Nonlinear Systems*. Prentice Hall, 2002.

[4] J.-j. E. Slotine and W. Li, *Applied Nonlinear Control*. Prentice Hall, 1991.

[5] L. Sciavicco and B. Siciliano, *Modelling and control of robot manipulators*. Springer, 2005.

[6] J. J. Craig, *Introduction to robotics*. Pearson Prentice Hall.

[7] C. G. Atkeson, A. W. Moore, and S. Schaal, "Locally Weighted Learning for Control," *Artificial Intelligence Review*, no. 11, pp. 75–113.

[8] M. Mistry, J. Buchli, and S. Schaal, "Inverse dynamics control of floating base systems using orthogonal decomposition," in *2010 IEEE International Conference on Robotics and Automation*, no. 3, 2010, pp. 3406–3412.

[9] O. Khatib, "A unified approach for motion and force control of robot manipulators: The operational space formulation," *Robotics and Automation, IEEE Journal of*, vol. 3, no. 1, pp. 43–53, 1987.

[10] J. Nakanishi, R. Cory, M. Mistry, J. Peters, and S. Schaal, "Operational Space Control: A Theoretical and Empirical Comparison," *The International Journal of Robotics Research*, no. 6, pp. 737 –757, 2008.

[11] J.-j. E. Slotine and W. Li, "On the Adaptive Control of Robot Manipulators," *International Journal of Robotics Research*, vol. 6, no. 3, pp. 43–50, 1986.

[12] V. I. Utkin, "Variable Structure Systems with Sliding Modes," *IEEE Transactions on Automatic Control*, vol. AC-22, no. 2, pp. 212–222, 1977.

[13] W.-h. Chen, D. J. Ballance, P. J. Gawthrop, S. Member, J. O. Reilly, and S. Member, "A Nonlinear Disturbance Observer for Robotic Manipulators," *IEEE Transactions on Industrial Electronics*, vol. 47, no. 4, pp. 932–938, 2000.

[14] A. Mohammadi, M. Tavakoli, H. J. Marquez, and F. Hashemzadeh, "Nonlinear disturbance observer design for robotic manipulators," *Control Engineering Practice*, vol. 21, no. 3, pp. 253–267, 2013.

[15] M. J. Kim and W. K. Chung, "Disturbance-Observer-Based PD Control of Flexible Joint Robots for Asymptotic Convergence," *IEEE Transactions on Robotics*, vol. 31, no. 6, pp. 1508–1516, 2015.

[16] S. Oh and K. Kong, "High Precision Robust Force Control of a Series Elastic Actuator," *IEEE/ASME Transactions on Mechatronics*, vol. 22, no. 99, pp. 71–80, 2016.

[17] E. Todorov and Weiwei L, "A generalized iterative LQG method for locally-optimal feedback control of constrained nonlinear stochastic systems," in *Proceedings of the 2005, American Control Conference, 2005.*, pp. 300–306.

[18] A. Sideris and J. E. Bobrow, "Solving Nonlinear Optimal Control Problems," *IEEE Trans. Autom. Control*, vol. 50, no. 12, pp. 2043–2047, 2005.

[19] S. Skogestad and I. Postlethwaite, *Multivariable Feedback Control*. John Wiley & Sons, 2001.

[20] M. Neunert, M. Giftthaler, M. Frigerio, C. Semini, and J. Buchli, "Fast Derivatives of Rigid Body Dynamics for Control, Optimization and Estimation," in *2016 IEEE International Conference on Simulation, Modeling, and Programming for Autonomous Robots*, 2016.

[21] S. J. Julier and J. K. Uhlmann, "Unscented Filtering and Nonlinear Estimation," in *Proceedings of the IEEE*, vol. 92, no. 3, 2004.

[22] R. Featherstone, *Rigid Body Dynamics Algorithms*. Springer.

[23] P. Lu, E. van Kampen, C. C. D. Visser, and Q. Chu, "Framework for state and unknown input estimation of linear time-varying systems," *Automatica*, vol. 73, pp. 145–154, 2016.

[24] E. A. Wan and R. van der Merwe, "The unscented kalman filter," in *Kalman Filtering and Neural Networks*, 2001, vol. 5, pp. 221–280.

[25] T. B. Cunha, "Hydraulic Compliance Control of the Quadruped Robot HyQ," Ph.D. dissertation, Istituto Italiano di Tecnologia, 2013.

[26] C. Semini, N. G. Tsagarakis, E. Guglielmino, M. Focchi, F. Cannella, and D. G. Caldwell, "Design of HyQ – a hydraulically and electrically actuated quadruped robot," *Journal of Systems and Control Engineering*, vol. 225, pp. 831–849, 2011.

[27] S. Schaal, "The SL Simulation and Real-Time Control Software Package," Tech. Rep., 2007.

[28] P. Lu, T. Sandy, and J. Buchli, "Nonlinear disturbance attenuation control of hydraulic robotics," in *IEEE International Conference on Robotics and Biomimetics*, 2018, pp. 1451–1458.